Soft Matter

PAPER

View Article Online
View Journal

Cite this: DOI: 10.1039/d6sm00071a

Photo-crosslinked pluronic hydrogels: micelle self-assembly and thermoresponsive behavior

Michel Habib,[ab] Joao Fragoso,[a] Christine Joly-Duhamel,[a] Jean-Pierre Habas,[a] Sylvain Catrouillet,[a] Audrey Tourrette,[b] Tahmer Sharkawi*[a] and Sebastien Blanquer*[a]

Amphiphilic block copolymers, such as pluronic triblock copolymers, are widely employed to engineer stimuli-responsive hydrogels for applications ranging from biomedicine to energy and food industries. In this study, we investigated how the self-assembly temperature of pluronic P123, P104, and F127 affects the crosslinking behavior and the temperature-dependent volume changes of the resulting hydrogels. Each pluronic bearing hydroxyl end-group was functionalized with methacrylic moieties to enable chemical photo-crosslinking and hydrogel formation. Before crosslinking, the impact of chain-end functionalization on micellar organization was evaluated using rheological measurements to map changes in the phase diagrams of the micellar solutions. The results revealed significant shifts in micellar organization for all three pluronics following methacrylation of the hydroxyl groups. Photorheological experiments further demonstrated that the micellar organization directly influenced the kinetics of chemical crosslinking: organized micellar states facilitated faster and more efficient photocrosslinking reactions. Temperature sweeps on the crosslinked systems showed that F127-MA, P123-MA, and P104-MA hydrogels exhibited significantly reduced thermoresponsiveness when crosslinked in an organized state. Finally, the rheologically observed thermal behavior was correlated with the hydrogels' swelling properties. The thermal responses of the pluronic hydrogels resulted in up to 30% water release when crosslinked in an isotropic state, compared to 20% when crosslinked in an organized state. These findings highlight the critical role of micellar organization in tuning the physicochemical properties of pluronic-based hydrogels.

Received 26th January 2026,
Accepted 14th May 2026

DOI: 10.1039/d6sm00071a

rsc.li/soft-matter-journal

1. Introduction

Pluronics are a family of triblock copolymers composed of alternating polyethylene oxide (PEO) and polypropylene oxide (PPO) blocks.[1–3] They have gained significant attention in scientific and industrial communities due to their unique behavior in aqueous solution as the concentration or the temperature increases. Specifically, pluronic polymers self-assemble into micelles in aqueous solutions above their respective (critical micelle concentration) CMC and/or critical micellar temperature (CMT).[4] Depending on the length of each block, pluronic micelles can further organize into different lyotrophic mesochanges with increasing concentration and/or temperature, forming gel-like materials.[5–7]

As a result, pluronic copolymers have found widespread use as thickeners and hydrogel matrices in cosmetics, while their excellent biocompatibility has further enabled broad applications in the biomedical field.[8–10] Thus, several studies have explored the combination of pluronic with biopolymers such as alginate, gelatin, chitosan, or hyaluronic acid. These studies share a common goal: to enhance the mechanical properties of these biopolymers by leveraging the micellar nature of pluronic, as well as its thermosensitive characteristics or its role as a drug carrier.[11–17] However, the micellar state of pluronic, once combined with a hydrogel, is rarely examined in these studies, and especially in photocrosslinked systems. As a result, there is a lack of understanding regarding how the self-assembly of pluronic micelles influences the properties of the photo-crosslinked hydrogels.

Traditionally, the phase boundaries of lyotropic mesophases can be determined using scattering techniques (SAXS & WAXS), whereas their nanostructures require the use of small angle neutron scattering experiments (SANS).[18–21] These measurements enabled the establishment of various mesophase geometries, typically including cubic, lamellar, and hexagonal structures.[22–24] Hence, using neutron scattering Wanka *et al.* succeeded in creating a series of phase diagrams for P104, L121, L122, P123, F127, PE6200, PE6400, P65, and F68 in

[a] *ICGM, Univ Montpellier, CNRS, ENSCM, Montpellier, France.*
E-mail: tahmer.sharkawi@umontpellier.fr, sebastien.blanquer@umontpellier.fr
[b] *CIRIMAT, Université de Toulouse, Toulouse INP, CNRS, Toulouse, France*

aqueous solutions, thus serving as references for the assembly of various types of pluronics.[25]

However, other more routine techniques, such as thermomechanical methods, have also proven effective at monitoring micellar organization in aqueous solutions. Specifically, rheological measurements (*e.g.*, temperature sweeps, oscillatory shear, and viscosity assays) offer sensitive detection of these physical changes. Thus, some reported studies in the literature correlated rheological temperature-sweep measurements with SAXS or SANS data, demonstrating that rheology reliably identifies pluronic phase transitions and complements SANS for characterizing lyotropic mesophases.[26–30]

In addition to establishing phase diagrams for these pluronics, rheological measurements enabled the rapid detection of their gelation behavior as a function of temperature and micellar self-assembly. These preliminary physicochemical studies are essential for developing thermoresponsive injectable hydrogels and for applications in 3D printing and bioprinting.[31–34]

Beyond their remarkable self-assembly properties, pluronics also exhibit advantageous structural and chemical features, notably due to the presence of hydroxyl end-groups. These functional groups can be leveraged in post-functionalization processes, offering a versatile strategy to tailor their properties.[35,36] However, even in the case of end-functionalization, the impact on the self-association of these functionalized pluronics remains insufficiently described. Contessi Negrini *et al.* studied the effect of telechelic norbornene functionalization of pluronic F127 on micellar dimensions and reported improved micelle stability upon functionalization.[37] Park *et al.* demonstrated this post-functionalization by introducing carboxyl groups into F127, imparting pH sensitivity. The inverted tube test method revealed a phase diagram shift toward higher concentrations, attributed to enhanced micelle hydrophilicity (*e.g.*, native F127 at 18% w/w gelled at >27 °C, whereas carboxylated F127 at >35 °C).[38] Similarly, Meng *et al.* grafted phosphorylcholine groups onto F107/F127, observing elevated gelation temperatures *via* rheology due to hydrophilic groups retarding PPO dehydration.[39] Finally, end-functionalization of pluronics with acrylic or methacrylic moieties, aimed at generating photo-crosslinked hydrogels, remains the most commonly reported modification in the literature. Hence, Di Biase *et al.* reported that at low concentrations, photo-crosslinking of F127 DA occurs predominantly within the micelles, leading to micellar crosslinks (nanogels) rather than bulk hydrogels.[40] At higher concentrations, Vandenhaute *et al.* synthesized photo-crosslinked hydrogels from methacrylated F127, L35, and L43, demonstrating a direct relationship between the self-assembling pluronic micelle's phase-transition temperature and the resulting hydrogel's thermoresponsive behavior.[41] Interestingly, Bhusari *et al.* demonstrated that the introduction of acrylate end-groups on pluronic F127 enhances the initial micellar aggregation, which then influences the structure and the mechanical properties of the photo-crosslinked gel.[42] Finally, by substituting an aqueous medium with an ionic liquid, López-Barrón *et al.* demonstrated that F127-DA self-assembles into micelles without disrupting their formation, and that subsequent photo-crosslinking of these micelles yields a highly viscoelastic network, highlighting that the micellar microstructure dictates the structure and mechanical properties of the resulting hydrogel.[43]

Overall, such previous studies lack a systematic and comparative investigation of the full transformation pathway, from native pluronic to methacrylated derivatives and ultimately to photo-crosslinked hydrogels, including an analysis of the thermoresponsive behavior of the resulting hydrogels, while maintaining consistent rheological and structural characterization across multiple concentrations. In addition, the relationship between the post-crosslinking micellar structure and its influence on thermoresponsiveness and volume-change behavior remains poorly understood, highlighting a significant gap in the field. Ultimately, although pluronic F127 has been the most extensively investigated, additional data are needed for other pluronic types, particularly concerning the structure–property relationships of functionalized polymers and their subsequent influence on photo-crosslinked hydrogels.

Hence, in this work, we establish clear links between self-assembly, swelling behavior, and rheological properties. This integrated approach provides a comprehensive understanding of how initial micellar organization and subsequent chemical modification govern the thermomechanical properties of the final thermoresponsive hydrogel. We systematically analyzed the thermomechanical behavior of pluronic F127, P123, and P104 before and after methacrylation, and following photo-crosslinking. Rheology served as a robust tool for tracking micellar organization changes between native and methacrylated copolymers, enabling phase diagram reconstruction. Furthermore, photo-rheology quantified how micellar configuration modulates crosslinking kinetics. Post-crosslinking, rheological temperature sweeps revealed the hydrogels' thermal responses, while swelling studies probed the dependence of thermoresponsiveness on the initial micellar state.

2. Materials and methods

2.1. Materials

Pluronics P123 (PEO_{20}–PPO_{70}–PEO_{20}), F127 (PEO_{106}–PPO_{70}–PEO_{106}), and methacrylic anhydride (MA) were purchased from Sigma-Aldrich. BASF chemicals generously donated pluronic P104 (PEO_{27}–PPO_{61}–PEO_{27}). Triethylamine (TEA) and dichloromethane (DCM) were purchased from Fisher Chemicals. Milli-Q water (conductivity = 18.2 mΩ cm at 23 °C) was used during this study. Lithium phenyl-2,4,6-trimethylbenzoylphosphinate (LAP) was synthesized as described by Majima *et al.*[44] All chemicals were used without further purification unless mentioned otherwise.

2.2. Methods

2.2.1 Pluronic methacrylation. Pluronic P104, P123, and F127 were functionalized *via* methacrylate grafting onto their terminal hydroxyl groups using identical reaction conditions. For each, 50 g of pluronic was dissolved in 100 mL DCM with

magnetic stirring (700 rpm) for 4 hours. Then, 20 equivalents of TEA relative to hydroxyl groups were added, followed by stirring for 30 minutes to ensure homogenization. Then, 10 equivalents of MA relative to the hydroxyl groups were added and the reaction was maintained at 25 °C for 24 hours. The product was then precipitated with petroleum ether, redissolved in water and purified by dialysis (500 Da MWCO membrane) against distilled water for 3 days (with water changes twice daily). The purified methacrylated pluronics were freeze-dried and stored at −18 °C until use.

2.2.2 ^{1}H-NMR. ^{1}H-NMR spectra were acquired on a Bruker Avance I 400 MHz spectrometer (64 scans, 5 s relaxation time) to determine the degree of methacrylation (DM). Samples were prepared by dissolving 5 mg of methacrylated pluronic in 1 mL of D_2O. The DM, defined as the percentage of hydroxyl groups converted to methacrylate moieties, was calculated by integrating the characteristic methacrylate proton peaks (1.95, 5.8, and 6.2 ppm) to the PPO methylene protons (–CH_3) at 1.07 ppm.

2.2.3 Rheological characterization and phase diagram determination. Rheological measurements were performed on a stress-controlled MCR302 rheometer (Anton Paar) using the standard Couette measuring system CC27/T200/SS. 15 mL of samples were used and covered with paraffin oil to prevent water evaporation. Temperature sweeps were performed from 5 to 85 °C at a heating rate of 2 °C min^{-1} under a constant load of 0.1 N, a strain of 1%, and a frequency of 1 Hz. These parameters were previously determined using stress sweep experiments, confirming that the measurements remained in the linear viscoelastic domain for all systems. Phase transitions were identified by monitoring changes in the storage (G') and loss (G'') moduli, with particular attention to initial micellization and subsequent mesophase organization.

Photo-rheology. Photo-crosslinking kinetics were analyzed using a Haake MARS 60 rheometer (Thermo Fisher Scientific) equipped with a 20 mm parallel plate geometry. Methacrylated pluronic solutions (25% w/w in water) containing 3.75% w/w LAP photoinitiator were prepared and equilibrated at 10 °C to maintain homogeneity. Measurements were performed under 400 s UV irradiation (0.5 mW cm^{-2} intensity, 320–480 nm filter) while maintaining a 0.5 mm gap. All tests were conducted under oscillatory shear conditions (0.1 N normal force, 1% strain, 1 Hz frequency), as confirmed by prior amplitude sweeps to be within the linear viscoelastic regime. The temperature was systematically varied to probe different organizational states identified in the phase diagrams.

2.2.4 Temperature sweeps on crosslinked systems. Following photo-rheological characterization, samples were cooled to 10 °C at 2 °C min^{-1}. Temperature sweeps were then performed from 10 to 80 °C (2 °C min^{-1} heating rate) under oscillatory shear conditions (0.1 N normal force, 2% strain, 1 Hz frequency, 0.5 mm gap) within the predetermined linear viscoelastic regime. The thermoresponsive behavior was monitored by tracking the temperature-dependent evolution of the storage (G') and loss (G'') moduli.

2.2.5 Hydrogel preparation. Photo-crosslinkable resins were prepared by dissolving methacrylated pluronics (25% w/w) with LAP photoinitiator (3.75% w/w relative to polymer) in ultrapure water. The precursor solution was injected into cylindrical Teflon molds (10 mm diameter × 4 mm height), covered with glass slides to prevent evaporation, and equilibrated for 1 h at either 10 °C or 50 °C to establish distinct micellar organizations before crosslinking. UV curing was performed for 10 min using a Bio-Link chamber (Thermo Fisher; 365 nm, 2–3 mW cm^{-2}). Post-crosslinking, hydrogels were subjected to 24 h aqueous purification (with twice-daily water changes) followed by vacuum drying at 45 °C for 24 h on Teflon sheets.

2.2.6 Cyclic swelling. The water uptake capacity was evaluated using dried hydrogel samples. Swelling experiments were conducted by cycling between 10 °C and 50 °C, with each temperature maintained for 24 hours to ensure equilibrium swelling. The swelling ratio (Q) was determined using eqn (1), where m_{swollen} represents the mass of the hydrogel sample after reaching equilibrium swelling. In contrast, m_{dry} represents the mass of the hydrogel after drying. The drying process involved placing the hydrogel in an oven set to 45 °C under vacuum for 24 hours to remove water from the network. All measurements were systematically performed on four independent samples (n = 4).

$$Q = \frac{m_{\text{swollen}}}{m_{\text{dry}}} \tag{1}$$

The thermally-induced water release was calculated as the percentage of water expelled from the hydrogels during heating, determined using eqn (2). All measurements were systematically performed on four independent samples (n = 4).

$$\text{Water release (\%)} = 100\left(1 - \frac{Q_{50\,^\circ\text{C}}}{Q_{10\,^\circ\text{C}}}\right) \tag{2}$$

3. Results and discussion

3.1. Elaboration of the pluronic methacrylation

Chemical crosslinking of pluronic hydrogels was achieved by methacrylate functionalization of the terminal hydroxyl groups (Fig. 1). ^{1}H-NMR confirmed successful modification, using the PPO block protons (1.08 ppm in D_2O) as the integration reference (174 for P104, 210 for P123 and F127). The degree of methacrylation ranged from 89–93% across all pluronic variants (P104, P123, and F127), as calculated from the characteristic methacrylate proton peaks (1.95, 5.8, and 6.2 ppm).

Before methacrylation, the R_H of F127-OH was evaluated to be close to 7.9 nm, which is slightly higher than that characteristic of P104-OH and P123-OH (4.5 and 4.6 nm, respectively). This size difference is logically correlated to the higher molecular weights of the different pluronics, which are 13 338 g mol^{-1} for F127-OH, 5900 g mol^{-1} for P104-OH, and 5820 g mol^{-1} for P123-OH.[45]

DLS experiments showed that methacrylation did not affect the hydrodynamic radius (R_H), as seen in Fig. S1. Table 1 lists

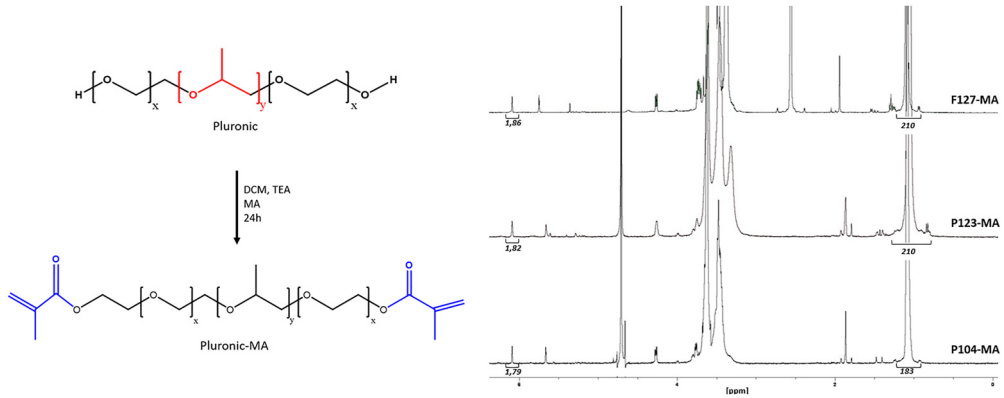

Fig. 1 Methacrylation of pluronic P104, P123, and F127 and ^{1}H-NMR spectra of the methacrylated products F127-MA, P123-MA, and P104-MA from top to bottom.

Table 1 Molecular weight, composition, hydrodynamic radius and aggregation temperature for each F127, P123 and P104 ($PEO_x - PPO_y - PEO_x$)

	M_w	x	y	PEO/PPO	R_H (nm)	$T_{aggregation}$ –OH (°C)	$T_{aggregation}$ –MA (°C)
F127	13 388	106	70	3.03	7.9	30	30
P123	5820	20	70	0.57	4.6	10	7
P104	5900	27	61	0.88	4.5	25	20

the values registered for all samples at 5 °C. Moreover, it can be seen that the aggregation of the unimers into micelles starts at 30 °C for F127-MA, 10 °C for P123-MA, and 25 °C for the P104-MA. Then, the aggregation temperature of F127-MA appears unaffected by methacrylation, in contrast to P123-MA and P104-MA, which decreased by almost 3 °C and 5 °C, respectively. This shows that methacrylation of the hydroxyl groups affects more hydrophobic pluronics like P123 and P104 rather than the more hydrophilic F127. The difference in aggregation temperature can be correlated with the length of the hydrophilic PEO segment and to the PEO/PPO ratio, given that the driving mechanism of aggregation is the dehydration of the PPO segment.[46–48] On one hand, by comparing F127 with P123, for a fixed PPO length, increasing the PEO segment will result in aggregation at higher temperatures due to increased chain hydrophilicity. On the other hand, comparing P123 with P104, for a similar M_w, a decrease in PEO/PPO will result in aggregation at lower temperatures.[49] Moreover, upon functionalization, the methacrylate groups are more dilute in the PEO segment of F127 than both PPO segments, thereby reducing their impact on the aggregation temperature.

3.2. Influence of end-functionalization on the pluronics phase diagrams

Above the critical micellar concentration (CMC), pluronic unimers self-assemble into micelles in water. The inner core is made of aggregated PPO blocks, while PEO sequences constitute the external corona. At higher temperatures and when the concentration is high enough, these micelles adopt different conformational structures (cubic, hexagonal, *etc.*) as previously revealed by neutron scattering.[25] Herein, we used rheological measurements to detect these different structures, following a previously published methodology.[50] The phases are assigned according to the predetermined phase diagrams in the literature. It should be noted that rheology does not directly determine the structural symmetry of the mesophases. However, transitions between unimers, micelles, and ordered phases typically produce distinct and reproducible changes in the viscoelastic response. These rheological signatures have previously been correlated with cubic and hexagonal organizations using scattering techniques such as SAXS or SANS. Therefore, in the present work, the identification of the different organizational states is inferred from rheological transitions and comparisons with phase diagrams reported in the literature, rather than being directly confirmed.

A schematic representation of the different micellar organizations is provided in Fig. 2 to guide the interpretation of the rheological transitions. This schematic illustrates the evolution from spherical micelles to ordered cubic packing and to hexagonally packed cylindrical micelles. The term ''cubic phase'' refers to the three-dimensional periodic packing of spherical micelles into a cubic lattice (such as body-centered or face-centered cubic arrangements), where each micelle occupies a well-defined position within a three-dimensional network, rather than to the individual shape of the aggregates. The term ''hexagonal phase'' refers to the two-dimensional hexagonal packing of cylindrical micelles, where each cylinder is surrounded by six neighbors, rather than to the individual shape of the aggregates.

Fig. 3, as an example, shows the results obtained with the three different copolymers in the native form and after methacrylation, at a polymer concentration of 30–35% w/w. By considering more precisely the case of P104-OH at 35% w/w for $T < 20$ °C, the G' and G'' values decrease with temperature. The aqueous solution consists of individual chains, called unimers, dissolved in water. Then, at $T = 20$ °C, the increase in both moduli indicates micellization due to the increased hydrophobic character of the PPO blocks and their subsequent aggregation. At $T = 25$ °C, G' increases and even overtakes G'' revealing the spatial organization of the micelles. The solution

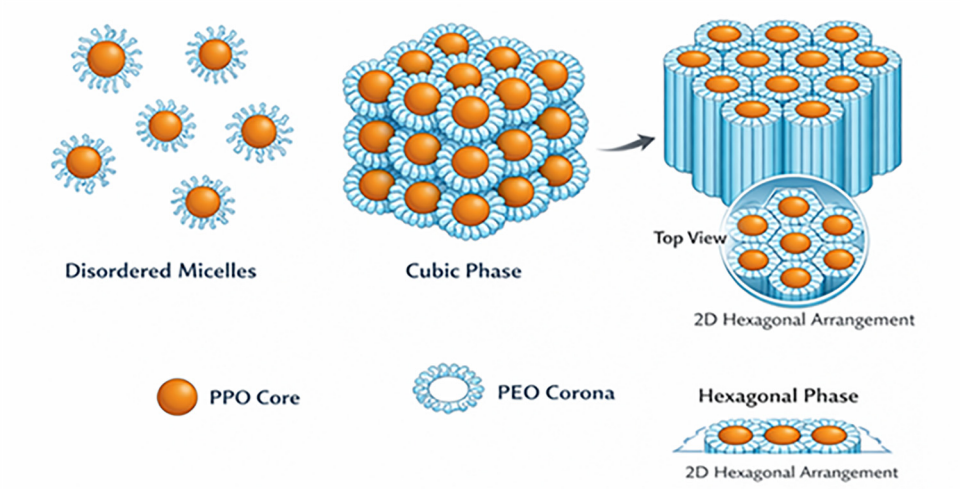

Fig. 2 Schematic representation of micellar organizations in aqueous pluronic systems. Disordered spherical micelles evolve toward ordered cubic packing and hexagonally packed cylindrical micelles with increasing temperature. These structures are schematic and based on literature descriptions of pluronic mesophases.

exhibits gel-like behavior, although it is well established that it is in fact a viscoelastic material with a long relaxation time. This ''gel'' state is observed until 47 °C. The consecutive decrease is consistent with a transition from a cubic-like organization to a hexagonal-like organization. This observed decrease in the elastic modulus can be attributed to changes in micellar packing and connectivity. In the cubic phase, micelles are arranged in a highly symmetric, three-dimensional network that maximizes inter-micellar contacts and mechanical load transfer, resulting in a higher modulus. Upon transition to the hexagonal phase, the micelles adopt a more anisotropic, one-dimensional arrangement, reducing the number of nearest-neighbor contacts and the effective crosslinking density of the network.

For higher temperatures ($T > 79$ °C), the significant increase in both G' and G'' values is provoked by solution demixing. Then, during the temperature sweep, several phases of P104-OH at 35% w/w were observed: unimer phase up to 20 °C, micellar phase up to 26 °C, cubic-like organization between 26 and 50 °C, and hexagonal-like organization between 60 and 79 °C, before demixing above 79 °C.[51,52] Similarly, for P123-OH at 37% w/w, the phases can be deduced as follows: unimer phase up to 8 °C, micellar phase between 8 and 12 °C, cubic phase between 12 and 45 °C, hexagonal phase between 45 and 60 °C and demixing above 60 °C.[53,54] For F127-OH 30% w/w the deduced phases are: unimer phase up to 17 °C, micellar phase between 17 and 23 °C, cubic phase between 22 and 87 °C and demixing above 87 °C.[55]

Fig. 3 shows that the grafting of methacrylic moieties at the PEO ends induces significant changes in the phase diagram of each pluronic studied, as reported by Park *et al.* with F127 modified with a carboxylic end group.[38] By comparing the order of magnitude of the storage and loss moduli, a correlation between the native and methacrylated pluronics was established to attribute the likely organizational states of the micelles. For P104-MA at 35%, the unimer phase is observed for $T < 15$ °C. The micellization occurs at a temperature between 15 and 20 °C. The divergence of both moduli due to the micellar organization is also shifted to a lower temperature (20 °C *versus* 26 °C). But the organized phase (likely cubic) is observed up to 40 °C, and a transition region consistent with hexagonal organization appears above 40 °C. In other words, it is more thermally stable than P104-OH at the same concentration. The transition of the consecutive phase is also more progressive. In the case of P123-MA at 37% w/w, the unimer phase is observed for $T < 30$ °C (against 20 °C). At the same time, micellization occurs between 30 and 35 °C (compared to 8 and 12 °C), followed by cubic organization between 35 and 52 °C (shifted from 12 to 45 °C) and hexagonal organization between 52 and 72 °C (from 60 and 79 °C for P123-OH). Similarly, for F127, the micellization occurs between 14 and 23 °C (compared to 16 to 22 °C), and the cubic organization phase is observed between 22 and 70 °C (compared to 23 to 87 °C for the native).

At first conclusion, the different pluronics functionalized with methacrylic moieties exhibit thermal responses that differ from those of the native copolymers. Such behavior is consistent with previous reports showing that end-functionalization of pluronics can shift micellization and organization boundaries without altering the fundamental self-assembly mechanism. In the present case, the methacrylate end-groups introduce a local perturbation at the chain extremities that may affect intermicellar interactions and packing constraints. In other words, for each studied copolymer, the functionalization of the end groups with methacrylic moieties provokes important changes in the thermal response of the native copolymers by modifying the hydrophilic/hydrophobic aspect of the amphiphilic chains. For P104 and P123, a shift to higher temperatures indicates a more stable cubic organization upon the introduction of hydrophobic methacrylic moieties at the chain ends due to the short PEO segments. However, for F127,

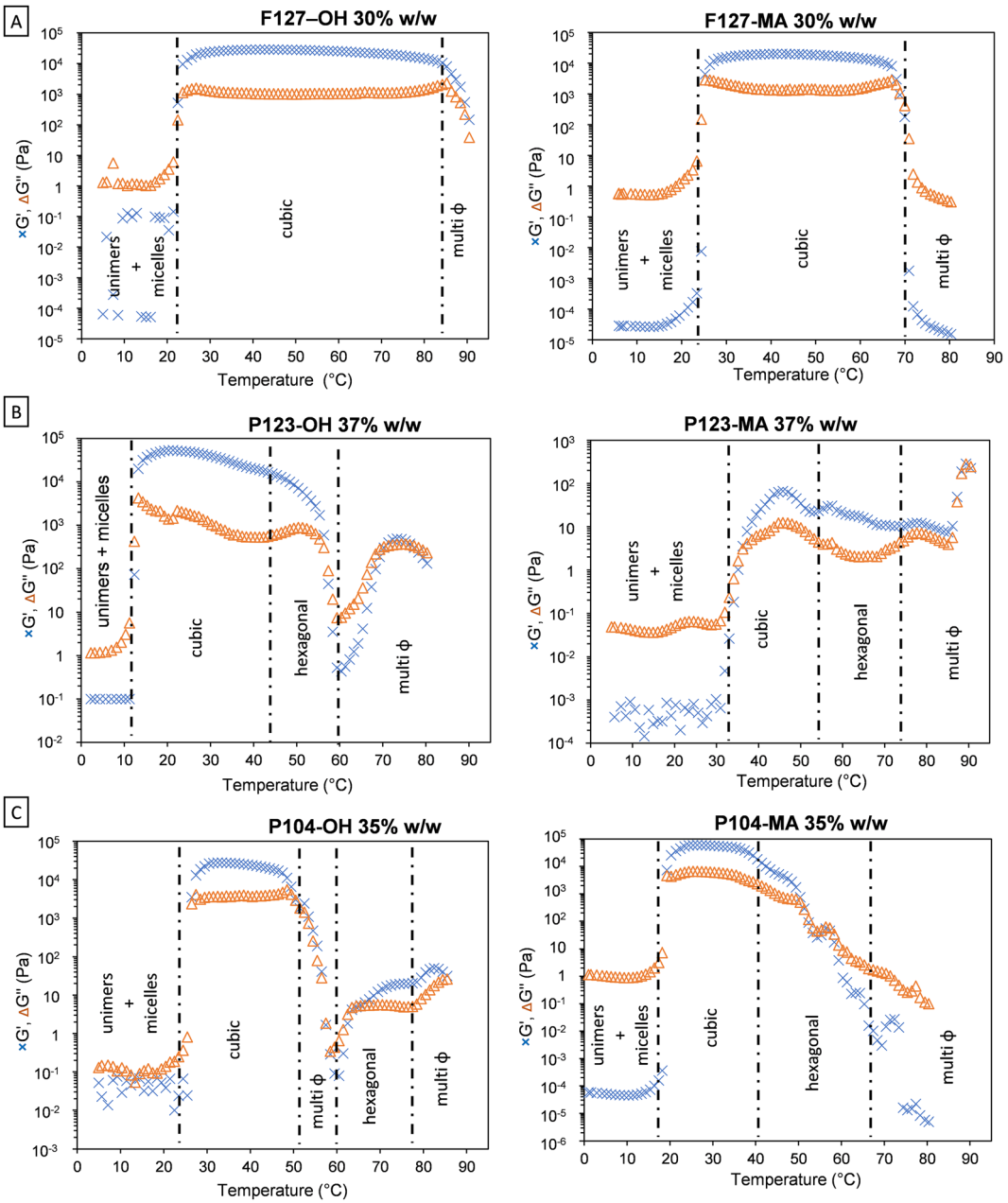

Fig. 3 Temperature sweeps of (A) P104-OH and P104-MA at 35% w/w, (B) P123-OH and P123-MA at 37% w/w, and (C) F127-OH and F127-MA at 30% w/w with the corresponding phases.

the cubic assembly phase becomes narrower and demixing occurs at a lower temperature upon methacrylation due to the increased length of the PEO segments.

The same measurements were done on native (–OH) and methacrylated (–MA) F127, P104 and P123 at various concentrations. From the rheograms (Fig. S2, S4 and S6), the phase diagrams of non-functionalized pluronic F127-OH, P123-OH, and P104-OH were obtained up to 40% w/w as represented in Fig. 4. Each phase transition corresponds to a significant change in the storage and loss modulus. The rheogram-derived phase diagrams of the non-functionalized pluronics are similar to those obtained by neutron scattering and reported in the literature, validating this methodology as a practical technique for detecting pluronic phase transitions.[25] It is interesting to note that for P123-OH below 30% w/w, no phase transitions can be detected using rheological measurements, which was not the case in the literature with scattering techniques. However, the samples become cloudy upon heating solutions of 20 and 30% w/w, as shown in Fig. S8, while remaining liquid. This effect may justify why X-ray or neutron scattering can detect a phase transition. At the same time, no detection was observed by rheology as the thermal response of the micelle assembly under these conditions did not manifest mechanically. Combining all the rheograms (Fig. S3, S5 and S7), we observe that the methacrylated pluronic exhibits a behavior

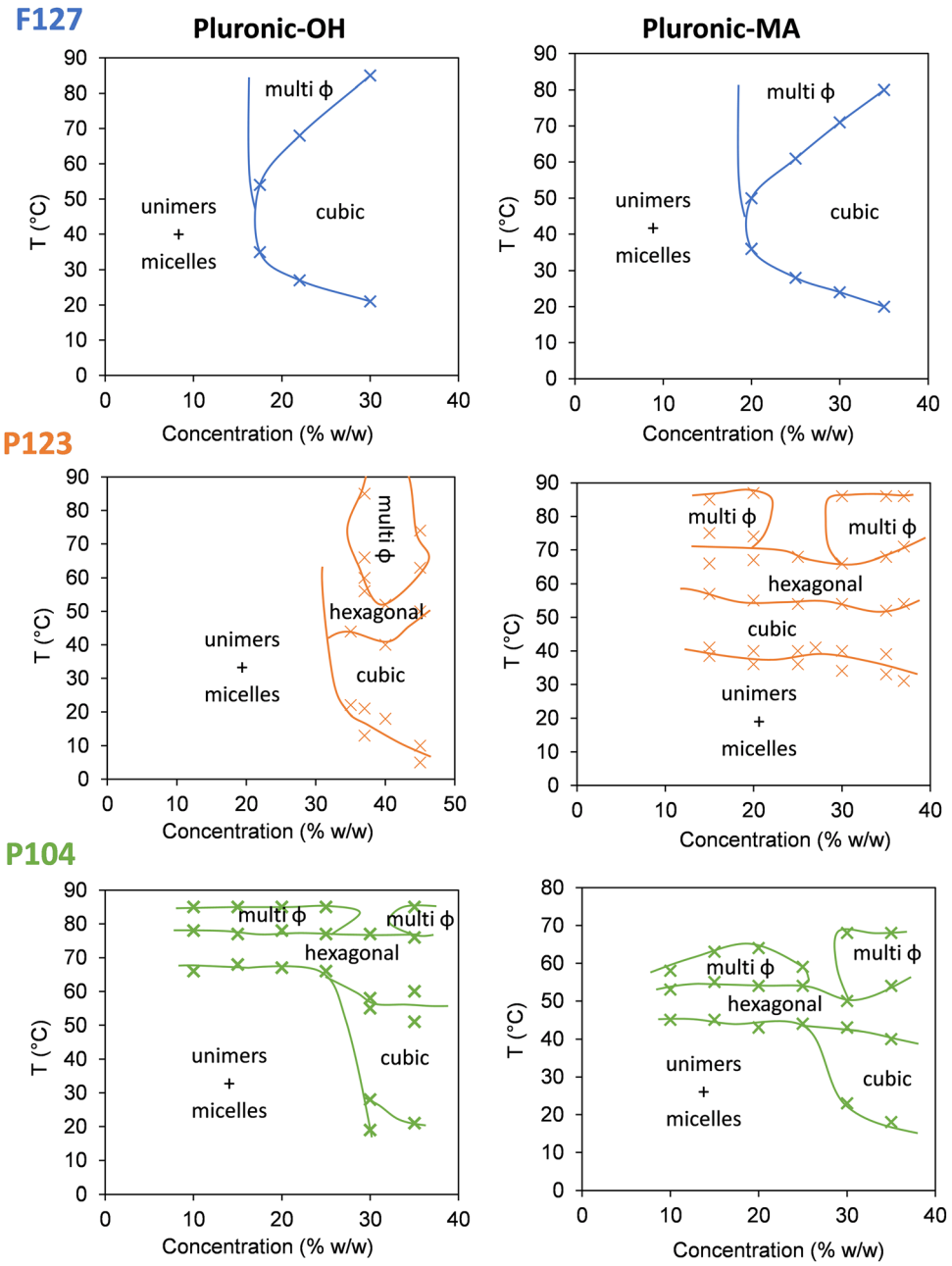

Fig. 4 Phase diagrams of native (–OH) and methacrylated (–MA) pluronics F127, P123, and P104 as obtained by rheological measurements.

similar to the non-methacrylated version with slight modifications. The F127-MA phase diagram shows a slight shift of the onset of self-assembly toward higher concentrations compared to its non-methacrylated counterpart, whereas P104-MA and P123-MA exhibit a shift toward lower concentrations relative to non-methacrylated P104 and P123, respectively. The influence of the hydrophobic methacrylic units on the pluronic chains can explain this shift. For P123 (PEO_{20}–PPO_{70}–PEO_{20}) and P104 (PEO_{27}–PPO_{61}–PEO_{27}), the ratio of PPO to PEO is significantly higher than that for F127 (PEO_{106}–PPO_{70}–PEO_{106}). Increasing the hydrophobicity by adding methacrylic moieties will shift the phase diagrams for P123 and P104 towards lower temperatures, indicating a favored micellar configurational change. Moreover, for F127, the phase diagram shifts slightly towards higher temperatures due to the longer chains being more hydrophilic, thereby hindering micelle assembly to a certain degree. Once more, it should be emphasized that the assignment of cubic and hexagonal mesophases is based on rheological signatures and comparison with literature phase diagrams. Complementary structural characterization techniques such as SAXS or SANS would be required for unambiguous identification of the mesophase symmetry.

3.3. Influence of micellar configuration upon photo-crosslinking

The photo-crosslinking behavior of methacrylated pluronics (25% w/w) was systematically investigated at temperatures

corresponding to distinct micellar organizational states. Photorheological measurements revealed a strong dependence of crosslinking kinetics on the initial micellar configuration, as evidenced by the temporal evolution of storage modulus (G') during UV irradiation (Fig. 5). It is first important to note that polymerization kinetics increase with temperature. However, in photopolymerization, the initiation step is primarily governed by light absorption and is therefore only weakly dependent on temperature, whereas the propagation step is more sensitive to temperature through its effect on chain mobility and diffusion. In the case of photochemical crosslinking of end-chain methacrylated oligomers, steric hindrance can limit chain growth, leading to relatively short kinetic chains and a reduced contribution of propagation.[56,57] Therefore, the rapid network formation observed likely reflects the pre-organized spatial arrangement of reactive methacrylate groups within these mesophases, which may facilitate efficient intermolecular bridging.

When crosslinking occurred in organized states (cubic-like or hexagonal-like organisation), all three pluronic derivatives reached modulus equilibrium within 60 seconds of UV exposure. In contrast, crosslinking in the unimer state (10 °C) required significantly longer irradiation times: 200 s for P104-MA and 320 s for both P123-MA and F127-MA. This kinetic difference arises from the disordered, mobile nature of unimers, in which the probability of encounters between methacrylate groups is reduced compared to organized micellar systems. In the unimer state, the pluronic copolymers are disordered and free to move, which could explain the longer time required to form stable chemical bridges between them. The micelles are more ordered at higher temperatures, and chemical crosslinking is facilitated and occurs faster.

3.4. Influence of photo-crosslinking on thermal responsiveness

Amphiphilic polymers can exhibit a thermal response upon temperature change. During heating, the polymer–polymer interactions can be favored in polymers with a lower critical solution temperature. Herein, we investigate by rheology the micellar configurational change as a means of inducing a thermal response in a photo-crosslinked hydrogel system. After methacrylation, upon heating, pluronics P104-MA, P123-MA, and F127-MA exhibited a conformational change in aqueous solution. The next step aims to determine whether the system can still exhibit a thermal response similar to that of uncrosslinked micelles following photo-crosslinking. Temperature sweep experiments were therefore performed on photo-crosslinked hydrogels

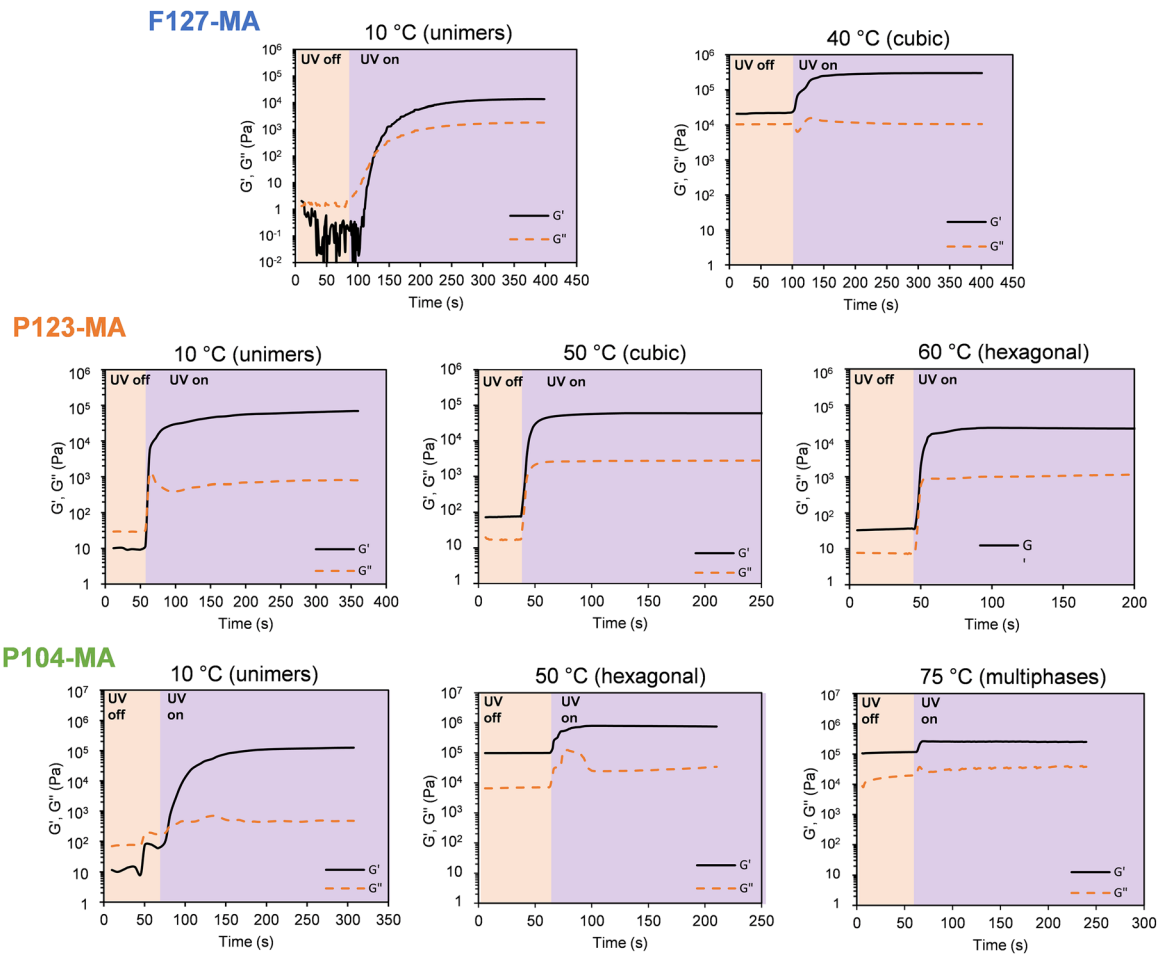

Fig. 5 Storage and loss modulus of F127-MA, P123-MA and P104-MA at 25% w/w during crosslinking under UV irradiation.

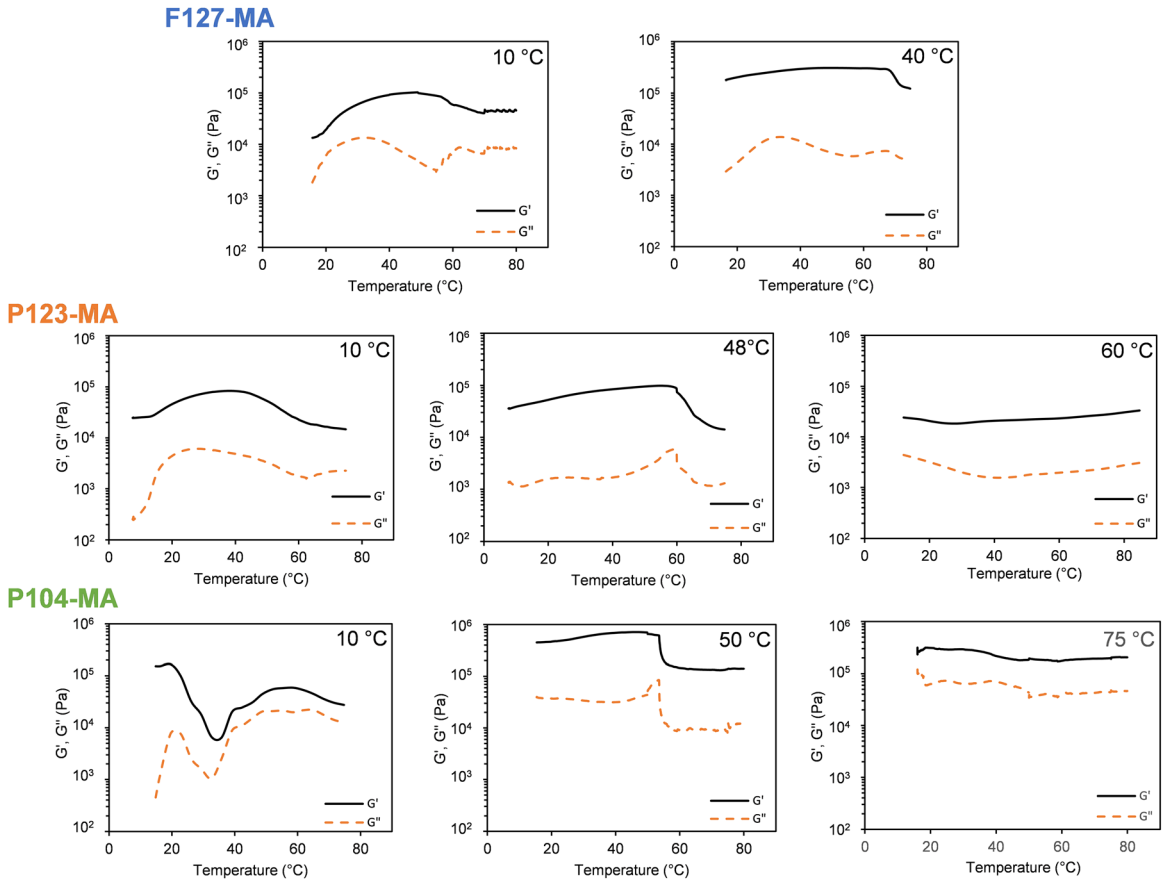

Fig. 6 Storage modulus of 25% w/w photo-crosslinked P104-MA, P123-MA and F127-MA under shear.

from different micellar configurations (unimer, cubic, and hexagonal phases), as defined by the phase diagrams of the modified pluronics. For these crosslinked systems, the objective is to interpret the rheological profiles and correlate them with the different microphase transitions. As shown in Fig. 6, distinct profiles are obtained depending on the state of organization at the time of photo-crosslinking.

In the case of hydrogels photo-crosslinked at 10 °C (*i.e.*, in the unimer state) for all three pluronics, the first observation is that the thermal response begins at temperatures lower than those expected from the phase diagrams of the methacrylated pluronics. The thermal response begins at lower temperatures than those expected from the phase diagrams of the methacrylated systems. For example, based on the phase diagrams at 25% w/w (Fig. 4), the first transition is expected at around 45 °C for P104-MA, 35 °C for P123-MA, and 30 °C for F127-MA, whereas in the crosslinked systems, the response starts at around 20 °C with reduced amplitude. This shift can be attributed to chemical crosslinking, which induces a more compact arrangement of polymer chains while still preserving the tendency of PPO blocks to aggregate. As a result, despite this temperature shift, the overall rheological profiles remain consistent with those of the uncrosslinked systems. (Fig. S3, S5 and S7), suggesting that the sequence of structural transitions is preserved but occurs at lower temperatures. At the same time, photo-crosslinking restricts chain mobility, limiting micellar rearrangements and reducing the amplitude of the variations in G' and G''.

In contrast, when the system is photo-crosslinked in an organized phase (cubic or hexagonal), the rheological behavior is markedly altered, notably with the disappearance of certain transitions. For samples photo-crosslinked in an intermediate state associated with a cubic phase (40 °C for F127-MA, 48 °C for P123-MA and 50 °C for P104-MA), the transition from the unimer to the cubic phase is no longer observed. Instead, a plateau appears until 68 °C, 55 °C and 60 °C for photo-crosslinked F127-MA, P104-MA, and P123-MA, respectively. This suggests that in such a network, the disruption of the pre-existing cubic organization does not occur under temperatures corresponding to the disordered unimer state, indicating that crosslinking in an organized phase prevents disorganization toward a less structured state due to network constraints. However, transitions toward higher levels of organization remain observable. A decrease in the elastic modulus, characteristic of a transition toward a hexagonal-like structure, is detected and is consistent with the rheological behavior of the pluronics. Hence, transitions occur at around 55 °C for P104-MA and 60 °C for P123-MA, in agreement with the expected cubic-to-hexagonal transition temperatures. Finally, when photo-crosslinking is performed in a more highly

organized state, such as a hexagonal-like phase, the values of G' and G'' do not show significant variation upon heating. This behavior can be explained by the fact that micellar associations are already established prior to crosslinking and become kinetically trapped within the network. As a result, the reduced chain mobility in a superior phase organization prevents any significant microphase transition over the explored temperature range and the hydrogels lose their thermal response due to the micelles being constrained from moving to a lower organizational state.

3.5. Volume change of hydrogels upon temperature variation

Pluronic cylindrical chemical hydrogels were prepared from 25% w/w methacrylated pluronic aqueous solutions in an 8 × 4 mm Teflon mold and photo-crosslinked at different organization states (unimer and cubic corresponding to 10 °C and 50 °C, respectively) in the presence of LAP as the photo-initiator. Gel content analysis revealed no significant dependence on the initial micellar organization state (Fig. S9). To determine the thermal response, the photo-crosslinked hydrogels were swollen in water at 10 °C for 24 h, corresponding to the unimer phase, then the hydrogels were left to swell in water at 50 °C above the transition temperature (unimer to cubic), which was determined earlier (Fig. 6). After 24 h, the hydrogels shrank, and the mass difference and the diameters between the two swollen states were recorded. The water release and the reduction in size (diameter) after heating are summarized in Fig. 7. Across all samples, whether crosslinked in the unimer or cubic state, a thermal response is observed through water expulsion ranging from 30 to 60%. In addition, hydrogels crosslinked in the unimer state exhibited a higher water-release profile when swollen at 50 °C, which can be explained by a greater degree of freedom in micelle mobility within the crosslinked matrix. The water release is evidenced by water expulsion (Fig. S10) and a reduction of the hydrogel size, with the most noticeable shrinkage occurring when the system is photo-crosslinked in the unimer state, as summarized in Fig. 7. This correlates with the previously shown rheological study, in which the thermal response is more pronounced in photo-crosslinked hydrogels below the micellization temperature.

4. Conclusions

This comprehensive investigation of methacrylated pluronics F127, P104, and P123 has revealed significant structure–property relationships governing their thermal behavior before and

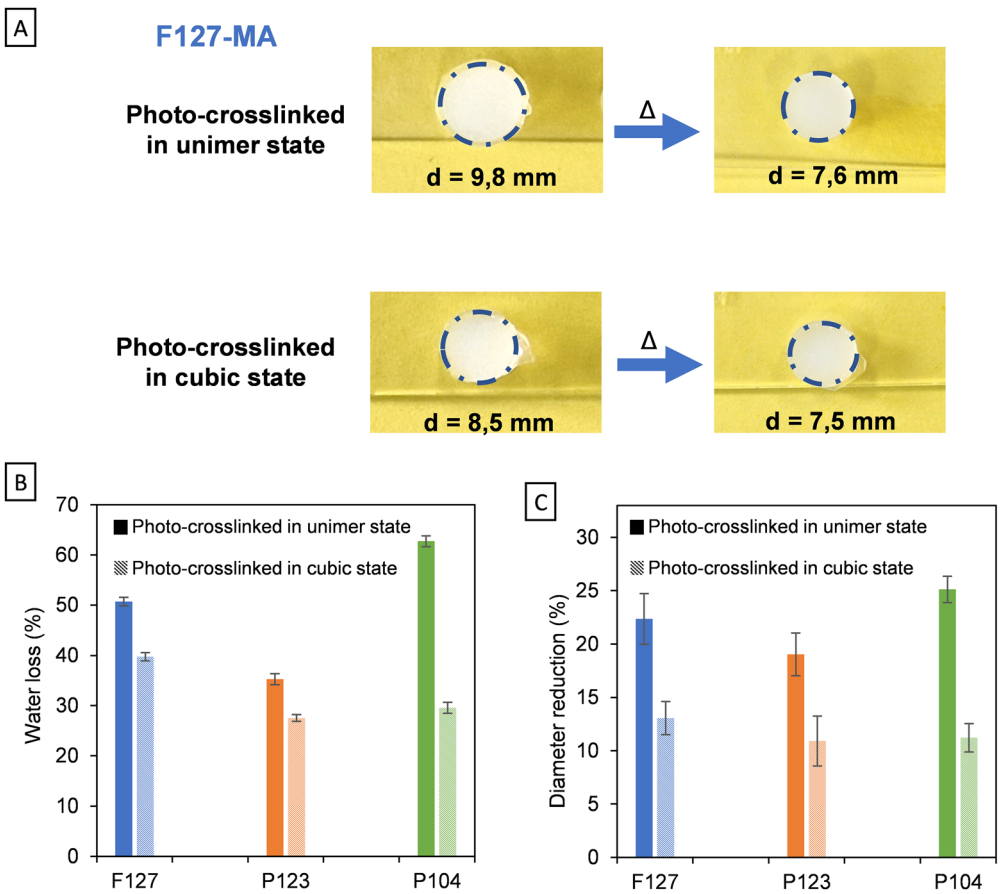

Fig. 7 (A) Physical representation of F127 25% w/w hydrogels swollen at 10 °C and 50 °C when crosslinked in unimer and cubic organizational states, and (B) water release and (C) diameter reduction of the hydrogels containing 25% w/w pluronics, photo-crosslinked under different conditions when heated from 10 °C to 50 °C.

after photo-crosslinking. The study demonstrates that methacrylation induces distinct shifts in phase diagrams – lowering transition concentrations for P104 and P123 while increasing them for F127 – reflecting the differential impact of hydrophobic methacrylate groups based on native copolymer architecture. Furthermore, when the micelles were in an organized state, the photo-crosslinking was observed to be faster and more efficient. Moreover, we noted that the thermal response of the hydrogels is highly dependent on the micelle's organizational state. When photo-crosslinking occurs in an organized phase (cubic or hexagonal), the thermal response becomes less prominent and is even lost in some cases, while photo-crosslinking in the unimer phase resulted in hydrogels with the most pronounced temperature response, resulting in a volume-changing hydrogel. Chemical photo-crosslinking does not limit the possible organization of the micelles to a higher state; however, it was observed to limit the disorganization to lower organizational states. These structure–property relationships position methacrylated pluronics as versatile precursors for designing thermo-responsive hydrogels with tunable properties. The demonstrated control over crosslinking kinetics and subsequent thermal behavior suggests particular promise for additive manufacturing applications, where spatial control of both network formation and stimulus-responsiveness could enable sophisticated 4D hydrogel constructs.

Author contributions

Michel Habib (investigation, methodology, writing original draft), Joao Fragoso (investigation, formal analysis), Christine Joly-Duhamel (formal analysis), Sylvain Catrouillet (formal analysis), Jean-Pierre Habas (validation, writing – review editing), Audrey Tourrette (project administration, supervision, validation, writing – review editing), Tahmer Sharkawi (conceptualization, project administration, supervision, validation, writing – review editing), Sebastien Blanquer (conceptualization, funding acquisition, project administration, supervision, validation, writing – review editing).

Conflicts of interest

The authors declare that they have no known competing financial interests or personal relationships that could have appeared to influence the work reported in this paper.

Data availability

Data will be made available on request.

Supplementary information (SI) includes DLS and rheology measurements of the different Pluronic diOH and diMA samples, as well as gel content and swelling properties of the photocrosslinked Pluronic hydrogels. See DOI: https://doi.org/10.1039/d6sm00071a.

Acknowledgements

This work has been supported by the Carnot Institute, ''Institut Carnot Chimie Balard Cirimat ICCBC''.

References

1 N. G. Andrade, I. O. Torquato, N. K. B. Lino, O. S. Pillaca-Pullo, N. V. P. Veríssimo, A. M. M. Maia, S. J. Brown, A. M. S. Jorge, V. C. Santos-Ebinuma, T. L. Greaves, I. C. Roberto, J. F. B. Pereira, C. O. Rangel-Yagui and A. M. Lopes, *J. Mol. Liq.*, 2025, **428**, 127530.
2 B. Chu, *Langmuir*, 1995, **11**, 414–421.
3 M. Newman, *Adv. Drug Delivery Rev.*, 1998, **32**, 199–223.
4 P. Alexandridis and A. Hatton'J, *Macromolecules*, 1993, **27**, 2414–2425.
5 R. K. Prud'homme, G. Wu and D. K. Schneider, *Langmuir*, 1996, **12**, 4651–4659.
6 B. Shriky, A. A. Vigato, A. F. Sepulveda, I. P. Machado and D. R. De Araujo, *Biophys. Rev.*, 2023, **15**, 475–496.
7 P. Zarrintaj, Z. Ahmadi, M. Reza Saeb and M. Mozafari, *Mater. Today: Proc.*, 2018, **5**, 15516–15523.
8 E. Gioffredi, M. Boffito, S. Calzone, S. M. Giannitelli, A. Rainer, M. Trombetta, P. Mozetic and V. Chiono, *Procedia CIRP*, 2016, **49**, 125–132.
9 A. Pitto-Barry and N. P. E. Barry, *Polym. Chem.*, 2014, **5**, 3291–3297.
10 P. Zarrintaj, J. D. Ramsey, A. Samadi, Z. Atoufi, M. K. Yazdi, M. R. Ganjali, L. M. Amirabad, E. Zangene, M. Farokhi, K. Formela, M. R. Saeb, M. Mozafari and S. Thomas, *Acta Biomater.*, 2020, **110**, 37–67.
11 S. Barberat, S. Nagarajan, M. Habib, A. Lebrun, N. Nieswic, M.-A. Lauzon, A. Aubert-Pouëssel, S. Blanquer and M.-N. Labour, *ACS Biomater. Sci. Eng.*, 2025, **11**, 5498–5511.
12 K. Singh, J. K. Wychowaniec, C. J. C. Edwards-Gayle, E. G. Reynaud, B. J. Rodriguez and D. F. Brougham, *J. Colloid Interface Sci.*, 2024, **660**, 302–313.
13 M. Abrami, I. D'Agostino, G. Milcovich, S. Fiorentino, R. Farra, F. Asaro, R. Lapasin, G. Grassi and M. Grassi, *Soft Matter*, 2014, **10**, 729–737.
14 J. García-Couce, M. Tomás, G. Fuentes, I. Que, A. Almirall and L. J. Cruz, *Gels*, 2022, **8**, 44.
15 Y. Liu, W. Zhou, Q. Zhou, K. Peng, A. Yasin and H. Yang, *RSC Adv.*, 2017, **7**, 29489–29495.
16 X. Wang, H. Mao, Y. Xiang, W. Ding, S. Zheng, Z. Wang, C. Bao and L. Zhu, *J. Mater. Sci.*, 2022, **57**, 17735–17750.
17 M. H. M. Nascimento, M. K. K. D. Franco, F. Yokaichyia, E. De Paula, C. B. Lombello and D. R. De Araujo, *Int. J. Biol. Macromol.*, 2018, **111**, 1245–1254.
18 G. Russo, G. Rossella Delpiano, C. Carucci, M. Grosso, C. Dessì, O. Söderman, B. Lindman, M. Monduzzi and A. Salis, *Eur. Polym. J.*, 2024, **204**, 112714.
19 F. Artzner, S. Geiger, A. Olivier, C. Allais, S. Finet and F. Agnely, *Langmuir*, 2007, **23**, 5085–5092.
20 M. J. Gaffney, Q. Han, K. Fox and N. Tran, *Gels*, 2025, **11**, 688.

21 H. Yardimci, B. Chung, J. L. Harden and R. L. Leheny, *J. Chem. Phys.*, 2005, **123**, 244908.
22 K. Mortensen, *J. Phys.: Condens. Matter*, 1996, **8**, A103–A124.
23 C. Perreur, J.-P. Habas, J. Peyrelasse, J. François and A. Lapp, *Phys. Rev. E:Stat., Nonlinear, Soft Matter Phys.*, 2001, **63**, 031505.
24 R. Linemann, J. Läuger, G. Schmidt, K. Kratzat and W. Richtering, *Rheol. Acta*, 1995, **34**, 440–449.
25 G. Wanka, H. Hoffmann and W. Ulbricht, *Macromolecules*, 1994, **27**, 4145–4159.
26 V. V. A. Fernández, N. Tepale, J. G. Álvarez, J. H. Pérez-López, E. R. Macías, F. Bautista, F. Pignon, Y. Rharbi, R. Gámez-Corrales, O. Manero, J. E. Puig and J. F. A. Soltero, *J. Colloid Interface Sci.*, 2009, **336**, 842–849.
27 J.-P. Habas, E. Pavie, C. Perreur, A. Lapp and J. Peyrelasse, *Phys. Rev. E:Stat., Nonlinear, Soft Matter Phys.*, 2004, **70**, 061802.
28 M. Zhang, M. Djabourov, C. Bourgaux and K. Bouchemal, *Int. J. Pharm.*, 2013, **454**, 599–610.
29 N. A. Di Spirito, N. Grizzuti, M. Casalegno, F. Castiglione and R. Pasquino, *Int. J. Pharm.*, 2023, **644**, 123353.
30 C. Chaibundit, N. M. P. S. Ricardo, F. D. M. L. L. Costa, S. G. Yeates and C. Booth, *Langmuir*, 2007, **23**, 9229–9236.
31 M. Müller, J. Becher, M. Schnabelrauch and M. Zenobi-Wong, *Biofabrication*, 2015, **7**, 035006.
32 S. Clerkin, K. Singh, D. Winning, I. Krupa, J. Crean, D. F. Brougham and J. K. Wychowaniec, *J. Mater. Chem. B*, 2025, **13**, 9351–9376.
33 J. M. White, A. Garza, J. J. Griebler, F. S. Bates and M. A. Calabrese, *Langmuir*, 2023, **39**, 5084–5094.
34 W. Shi, S. Jang, M. A. Kuss, O. A. Alimi, B. Liu, J. Palik, L. Tan, M. A. Krishnan, Y. Jin, C. Yu and B. Duan, *ACS Nano*, 2024, **18**, 7580–7595.
35 C. F. De Freitas, J. De Araújo Santos, D. S. Pellosi, W. Caetano, V. R. Batistela and E. C. Muniz, *Biomater. Adv.*, 2023, **151**, 213484.
36 D. Sil, M. Kumar, D. Kumar, V. Saini, B. D. Kurmi, R. R. Pal and S. Srivastava, *Eur. Polym. J.*, 2025, **239**, 114259.
37 N. Contessi Negrini, H. Sun and A. D. Celiz, *Biomater. Sci.*, 2026, **14**, 518–530.
38 S. Y. Park, Y. Lee, K. H. Bae, C. Ahn and T. G. Park, *Macromol. Rapid Commun.*, 2007, **28**, 1172–1176.
39 S. Meng, Z. Guo, Q. Wang, Z. Liu, Q. Wang, W. Zhong and Q. Du, *J. Biomater. Sci., Polym. Ed.*, 2011, **22**, 651–664.
40 M. Di Biase, P. De Leonardis, V. Castelletto, I. W. Hamley, B. Derby and N. Tirelli, *Soft Matter*, 2011, **7**, 4928.
41 M. Vandenhaute, J. Schelfhout, S. Van Vlierberghe, E. Mendes and P. Dubruel, *Eur. Polym. J.*, 2014, **53**, 126–138.
42 S. Bhusari, M. Hoffmann, P. Herbeck-Engel, S. Sankaran, M. Wilhelm and A. Del Campo, *Soft Matter*, 2024, **20**, 1320–1332.
43 C. R. López-Barrón, R. Chen, N. J. Wagner and P. J. Beltramo, *Macromolecules*, 2016, **49**, 5179–5189.
44 T. Majima, W. Schnabel and W. Weber, *Makromol. Chem.*, 1991, **192**, 2307–2315.
45 K.-C. Shih, Z. Shen, Y. Li, M. Kröger, S.-Y. Chang, Y. Liu, M.-P. Nieh and H.-M. Lai, *Soft Matter*, 2018, **14**, 7653–7663.
46 X. Liang, C. Guo, J. Ma, J. Wang, S. Chen and H. Liu, *J. Phys. Chem. B*, 2007, **111**, 13217–13220.
47 M. Ben Henda and A. Gharbi, *Polym. Sci., Ser. A*, 2017, **59**, 624–634.
48 Y. Su, J. Wang and H. Liu, *J. Colloid Interface Sci.*, 2002, **251**, 417–423.
49 C. Guo, J. Wang, H. Liu and J. Chen, *Langmuir*, 1999, **15**, 2703–2708.
50 J.-P. Habas, E. Pavie, A. Lapp and J. Peyrelasse, *Rheol. Acta*, 2008, **47**, 765–776.
51 E. B. Figueroa-Ochoa, L. M. Bravo-Anaya, R. Vaca-López, G. Landázuri-Gómez, L. C. Rosales-Rivera, T. Diaz-Vidal, F. Carvajal, E. R. Macías-Balleza, Y. Rharbi and J. F. A. Soltero-Martínez, *Polymers*, 2023, **15**, 2551.
52 S. Dos Santos, B. Luigjes and L. Piculell, *Soft Matter*, 2010, **6**, 4756.
53 Y. Zhao, X. Chen, C. Yang and G. Zhang, *J. Phys. Chem. B*, 2007, **111**, 13937–13942.
54 G. E. Newby, I. W. Hamley, S. M. King, C. M. Martin and N. J. Terrill, *J. Colloid Interface Sci.*, 2009, **329**, 54–61.
55 K. Mortensen, W. Batsberg and S. Hvidt, *Macromolecules*, 2008, **41**, 1720–1727.
56 A. K. Burkoth and K. S. Anseth, *Macromolecules*, 1999, **32**, 1438–1444.
57 F. P. W. Melchels, A. H. Velders, J. Feijen and D. W. Grijpma, *Macromolecules*, 2010, **43**, 8570–8579.

